Design of multilayer optical thin-films based on light scattering properties and using deep neural networks

Marin Fouchier, Myriam Zerrad, Michel Lequime, Claude Amra

Research Article | Vol. 29, No. 20 / 27 Sep 2021 / Optics Express 32627
Optics EXPRESS

Design of multilayer optical thin-films based on light scattering properties and using deep neural networks

MARIN FOUCHIER,[1,2,*] MYRIAM ZERRAD,[1] MICHEL LEQUIME,[1] AND CLAUDE AMRA[1]

[1]Aix Marseille Univ, CNRS, Centrale Marseille, Institut Fresnel, Marseille, France
[2]Centre National d'Etudes Spatiales, Toulouse, France
[*]marin.fouchier@fresnel.fr

Abstract: Despite limiting the performance of multilayer optical thin-films, light scattering properties are not as yet controllable by current design methods. These methods usually consider only specular properties: transmittance and reflectance. Among other techniques, design of thin-film components assisted by deep neural networks have seen growing interest over the last few years. This paper presents an implementation of a deep neural network model for light scattering design and proposes an optimization process for complex multilayer thin-film components to comply with expectations on both specular and scattering spectral responses.

1. Introduction

In the face of growing expectations in optical thin-film synthesis, several analytical and numerical tools have been developed for designing multilayer structures optimized for their specular properties, namely reflectance and transmittance. These techniques efficiently address the design problem and generate complex coatings up to several hundreds of layers with extreme levels of performance. Now well understood are classical optical responses such as narrow-band filters [1], broad-band antireflective [2], high reflectivity mirrors, phase dispersion mirrors [3], notch filters [4], etc. The thin-film community has also addressed design challenges which are not dedicated to scientific applications but demonstrate the ability to synthetize any fully arbitrary spectral response [5]. Nevertheless, design methods do not usually accurately take into account the scattering losses of the components even though this is now one of the main limiting factors for new generations of high-performance optical coatings. For example, for Space applications [6–11] or interferometric detection of gravitational waves [12–26], scattering losses of 10^{-5} or 10^{-6} are already significant. The metrology and the modeling of these scattering losses has been subject of several studies but none of them has been able to address the inverse problem with satisfying results yet. One of the rare techniques that has been implemented is based on anti-scattering layers to reduce and even eliminate scattering effects [27,28]. However, these techniques only work for specific coatings at single wavelengths and may be highly complex, e.g., using oblique deposition of fully correlated layers. As an alternative to classical design techniques, this paper proposes the implementation of a model based on deep neural networks to perform a first step toward an efficient design strategy based on light scattering. At this step, our main objective is not to propose a new learning model, but to couple existing deep learning tools with an electromagnetic model of scattering losses in optical coatings [29] that we have developed. To our knowledge, it is the first time that such a design is made possible, and it offers new perspectives for the design and manufacturing of high-performance optical coatings.

#437789 https://doi.org/10.1364/OE.437789
Journal © 2021 Received 14 Jul 2021; revised 30 Aug 2021; accepted 31 Aug 2021; published 24 Sep 2021

Optics EXPRESS

2. Specular based thin-film design

The design of thin-film interference filters has been a key topic for years and has led to successful and widely used techniques [30,31]. Among these, in 1982 Tikhonravov proposed a powerful algorithm called *needle* [32,33]. Given a starting design and some fixed constraints on the expected specular spectral response, the *needle* method converges reliably to good solutions. Even very complicated optical responses can be synthesized with fine adjustments. This well-known design problem involves many parameters: the thickness and the material properties of each layer (refractive index, spectral dispersion), the number of layers, the total thickness, etc. The *needle* algorithm is widely used in the thin-film community for both research and industrial applications. As with any numerical computation, the increasingly available computational power has also facilitated its implementation and use. The calculation of the specular spectral response of any well-known multilayer structure is now very fast and requires little in the way of computational resources using the complex admittance method, for example [29,31]. This computational step lies at the core of the design process, where each intermediate or final solution and its goodness of fit to the expected response is evaluated with a call to this function.

The *needle* technique is known as a non-global optimization method because it is unlikely to reach the global optimum for the problem being solved. Over the last few decades, substitutes have been proposed for optical thin-film design; among these are genetic algorithms [34,35], differential evolution [36,37], particle swarm optimization [38], simulated annealing [39], clustering global optimization [40] and more recently, deep neural networks [41,42]. Encouraging results have been obtained in some cases but usually for very specific problems, with many fixed parameters and a restricted number of layers (usually less than 40). The problems tackled are not always representative of the state-of-the-art challenges. None of these methods has yet outperformed the *needle* algorithm but they do present some promising features and perspectives.

3. Light scattering in optical thin-film coatings

Due to their numerous physical interfaces and their roughness, thin-film coatings present scattering losses which can drastically alter their performance for demanding applications such as illustrated in section 1. Hence, the computation of light scattering properties has been intensively studied over the last two decades. The spectral and angular responses of the field scattered by any optical coating can be successfully predicted under nominal conditions [29] but the inverse problem has remained unresolved until now. In a few words, the scattered light is induced by the coupling of the illumination field and the microroughness of the interfaces between each layer. Each of them is represented as a surface courant which is propagated in the far field through the coating, in every propagative direction and for every wavelength. Numerical results show an excellent agreement with metrology even for hundreds of layers [11,43]. The calculation considers the structural features of the multilayer (thickness of each layer, materials and roughness of each interface), the conditions of illumination (angle of incidence, wavelength and polarization) and the measurement conditions (scattering angle). It outputs the values of the scattering function ARS (Angle Resolved Scattering). This calculation is far more complex than the specular case. As an illustration, consider a structure with N layers of respective thicknesses $e_{p\in[[1;N]]}$ and materials $n_{p\in[[1;N]]}$, where n_p can be extracted from a database of at least two materials. The algorithms described in [29] for the computation of the specular spectral transmittance $T(\lambda,\ i)$, reflectance $R(\lambda, i)$ and ARS functions in transmission $ARS_T(\theta, \lambda, i)$ and in reflection $ARS_R(\theta, \lambda, i)$ require the following numbers of numerical operations:

$$N_{specular} = [N + 2] \times N_\lambda \times N_i$$

$$N_{scattering} = [[7\ \times N + 2] \times N_\theta + N] \times N_\lambda \times N_i$$

Optics EXPRESS

where N_λ is the number of wavelengths λ, N_i the number of angles of incidence i and N_θ the number of scattering angles θ. The calculation of the scattering responses includes calculation of the specular ones. All these properties are intrinsically connected, meaning that it is not possible to control them independently. Any change made to the main parameters of the optical coating will affect both specular and scattering properties in some way. As a numerical example, let us evaluate the number of operations required for the computation of the optical responses of a 60-layer filter ($N = 60$) in the visible range (from 400 nm to 1 µm every nanometer, $N_\lambda = 600$), at one angle of incidence ($N_i = 1$) and for a scattered intensity sampled every degree from 0° to 180° ($N_\theta = 90$, due to the parallel calculation in reflection and transmission). Computation of the specular coefficients requires $N_{Specular} = 37,200$ operations and the scattering computation needs $N_{Scattering} = 22,824,000$ operations, i.e., 600 times larger in this case. The evaluation of scattering properties requires significantly more computational power and involves more variables than for the specular case. The ARS function is angularly and spectrally dependent and therefore involves many more parameters.

4. Design using deep neural networks

There are no analytical solutions for both specular and scattering inverse design problems. The proven techniques developed for specular based design rely on a simplex linear optimization of a target criterion, leading to the identification of local optima. This approach is no longer realistically possible for the scattering response due to the heavy computation required and the large number of variables involved. Hence, we propose a numerical inverse problem solution based on deep neural networks: these are non-linear models and able to handle large multidimensional problems.

Promising results have been obtained in photonic design over the last five years, benefiting from developments in artificial intelligence and machine learning. There is a growing interest in deep neural networks (*DNN*) due to their ability to solve many problems and approximate any function [44]. Using a large set of examples describing the problem to be tackled, the program learns to generalize the features and make accurate predictions. The design of thin-film structures based on their specular properties has been widely studied and is a so-called *one-to-many* problem. For *one* given spectral response there are *many* possible multilayer thin-films that could be suitable solutions. This issue prevents the training of a *DNN* in proposing a design in a forward manner. In this context, solution of the inverse problem usually requires several networks or a few tricks to circumvent this issue, e.g. the back-calculation approach developed by Peurifoy [45] or the tandem network method introduced by Liu [41]. To our knowledge, only an implementation of a Mixture Density Network was successful in designing thin-films in the forward sense [42] because this specific model is not deterministic but provides probability distributions as output. Moreover, suitable and well-designed machine learning programs offer huge increases in computational speed compared with analytical calculations. Very simple design problems can even be solved by computing all possible solutions [46]. It is also worth mentioning that many other machine learning and deep learning techniques have been reported and reviewed for general photonic inverse problem solution [47–51]. These techniques involve different implementations and frameworks: generative adversarial networks [52,53], autoencoders [54], metasystems which combine several networks and optimization tools in a single process [55], etc. But they are not always suitable for the design of optical thin-films. Finally, Trubetskov has proposed a method called *deep search* to help convergence of the *needle* algorithm and avoid some local optima; the author has tested it on very complex design problems, but without much detail on its implementation or operational process [56].

The design problem based on light scattering is formulated in the same way and faces the same *one-to-many* problem. For a sake of simplicity and to minimize the number of variables, the spectral response that we consider is that of Total Integrated Scattering in transmission

Optics EXPRESS

(TIS_T), defined as the angular integration of the ARS_T function. The TIS_T sums all the angular contributions of the scattered fields in the transmitted half-space:

$$TIS_T(\lambda, i) = 2\pi \int_{\theta=1^\circ}^{90^\circ} ARS_T(\theta, \lambda, i) sin(\theta) d\theta \quad (1)$$

For a fixed angle of incidence i, the function counts only one variable λ whereas its calculation requires knowledge of the angular variations of the ARS function in transmission. The spectral response under investigation is therefore 1-dimensional, just as for the specular case. A similar analysis can of course be done in the reflected half-space. In the next sections, the angle of incidence is fixed to the value of 5°, the illumination is unpolarized and the scattering functions are sampled every degree from 1° to 90° in the transmitted half-space. The materials are specified for each implementation (SiO_2 and Nb_2O_5) and their dispersive refractive index values are taken from the literature [57,58]. At last, to minimize the number of variables, the microroughness is considered unchanged whatever the design. In this context, the only input of the model is a vector of layers thickness values of the component under investigation, the output is a vector of the TIS_T values sampled over a specified wavelength range.

5. Design framework

The framework of our design technique is inspired by that presented by Chen and Gu [59] and illustrated at Fig. 1. The process uses two *DNNs*: a *predictor* and a *designer*. The *predictor* is a forward *DNN* trained to predict the spectral response (output) of a given multilayer thin-film structure (input). The number of layers of the multilayer structure is fixed and the input features are the layer thickness values. The optical refractive indices are also fixed.

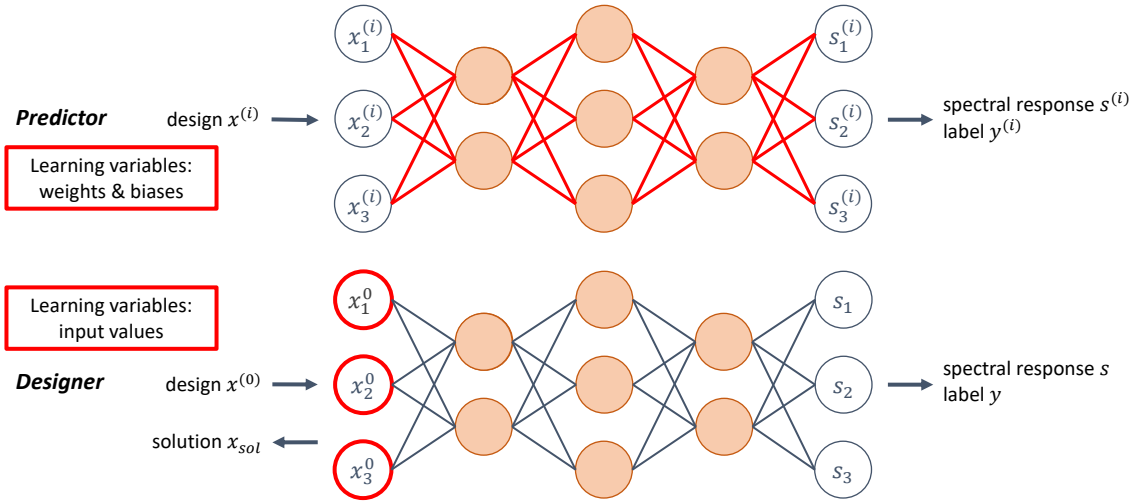

Fig. 1. *predictor* & *designer* design framework. The *predictor* is trained to predict spectral responses of given designs. The *designer* is a frozen copy of the *predictor* (fixed weights and biases); the training only modifies the input values.

The learning variables of the *predictor* are the weights and biases of its hidden layers. Once the *predictor* is trained, the network is copied to form the *designer*. The weights and biases of the hidden layers of the *designer* are frozen, and the learning variables are the input values. The training of the *designer* requires only one example: a random input vector and a hand-picked target output spectral response. The training process finely adjusts the input thicknesses and

Optics EXPRESS

tends to minimize the error between the prediction of the network and the given target response. All the layers are fully connected (their number and size vary according to the problem to be solved), separated by ReLU (Rectified Linear Unit) or leaky ReLU activation functions; the parameters are updated with the Adam optimizer. The loss function is a *Mean Squared Error* (MSE) function. The input data is standardized so that the values lie between 0 and a few units, e.g., 2 or 3. The spectral responses lie between 0 and 1 but the scattering levels are usually less than 10^{-2}, which is difficult to evaluate on a linear scale. Logarithm ($-\log_{10}(y)$) is taken on the output label data y to help the model to differentiate between low output values; the resulting output labels typically sit between 0 and n, with 10^{-n} the lowest level for the TIS. Typically, $n = 5$ or 6 for classical filtering applications. The whole model is implemented in MATLAB.

6. Application: designing a coating under light scattering control

For our first implementation, we consider structures of 20 alternating layers of SiO_2 and Nb_2O_5. The alternation is fixed and the layer on the top (interfacing the superstrate and illuminated by the incident field) is always of high index material (i.e., Nb_2O_5). The 20 input features are the 20 thickness values of the layers, varying from 60 nm to 120 nm. The training of the *predictor* uses a dataset of 50,000 examples, the input vectors are randomly generated and the corresponding scattering response output values are uniformly sampled over 201 points between 400 nm and 800 nm. Generating this dataset takes about 4 hours on a 24-core Intel Xeon Silver processor. The set is split into a training set (80% of the examples) and a validation set (20%). The *predictor* network has 5 fully connected hidden layers (with respectively 500, 500, 500, 201 and 201 units) separated by ReLU layers. The 128-epoch training on an Intel Core i5 processor lasts about 40 minutes. The *Root Mean Squared Error* (RMSE) at the final iteration is close to 0.84 on the training set and 1.09 on the validation set. The architecture of the *designer* is the same as the *predictor*, and the weights and biases are copied from the *predictor*. The design process uses a hand-picked target spectral response y (from the validation set) which is associated with a randomly initialized input vector $x^{(0)}$. The training of the network only modifies the values

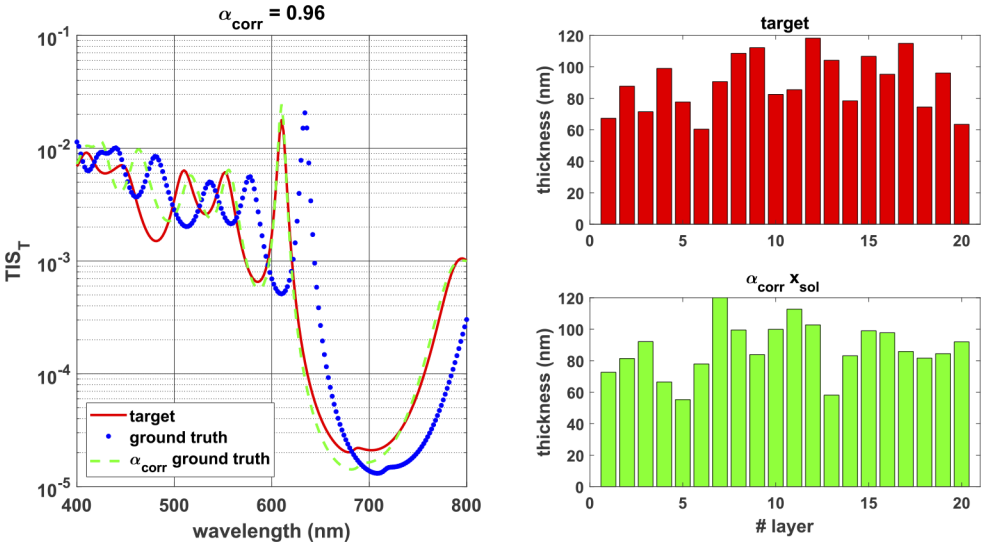

Fig. 2. Design process on a 20-layer thin-film structure. Good agreement between the target spectral response (red line) and the corrected predicted solution (green dashed line) which is shifted from the uncorrected solution (blue points). The correction coefficient is 0.96, meaning that the design process made a 4% error on the solution prediction.

Optics EXPRESS

of the input vector parameters to minimize the *MSE* of the prediction compared with the target and converges to the solution x_{sol}. This design approach benefits from the high computational speed of the *DNN* and the gradients computed by backpropagation. A training of 1024 epochs is usually enough to converge to a suitable solution. Finally, the solution is assessed using an exact analytical computation of the spectral response, called *ground truth*, to ensure that it complies with the prediction of the *designer*. As the *designer* is trained on only one example, the process is repeated for every new target. The optimized structures differ from the expected one but the requirements are generally respected. This confirms that several structures could have similar spectral responses.

In some cases, there is a slight spectral shift between the target and the ground-truth. This can be explained by a minor prediction error made by the *predictor*. Then the *designer* reproduces this discrepancy into a constant error over all thickness value predictions. It could be corrected by a further training of the *predictor* on more examples, but it is also possible to remedy this by multiplying all the thickness values of the solution x_{sol} by a correction coefficient α_{corr} close to 1. Tuning α_{corr} transforms the problem into a 1-dimensional optimization. Figure 2 presents an example of inverse problem solution with the aforementioned framework.

7. Application: refining a complex coating under light scattering control

There are a few caveats about the method mentioned above because it is dedicated to a single configuration (fixed number of layers and materials) with a few layers and a very narrow thickness variance, often less than the well-known $\lambda/4$ threshold value used in many thin-film structures. However, the more layers there are, the more complex is the optical response. Designing from scratch a complex multilayer structure, with several dozens of layers, very large thickness variance and under light scattering control, seems impossible in this context. Even the *needle* algorithm usually exploits starting designs and makes use of well-known efficient structures for designing complex specular functions. Our model has no knowledge of these reliable structures and outputs unconventional solutions to be refined or adjusted. This first simple implementation is unlikely to lead to the solution of complex design problems. Finally, the specular and scattering properties are intrinsically connected and adjustments made on one will necessarily affect the other. It

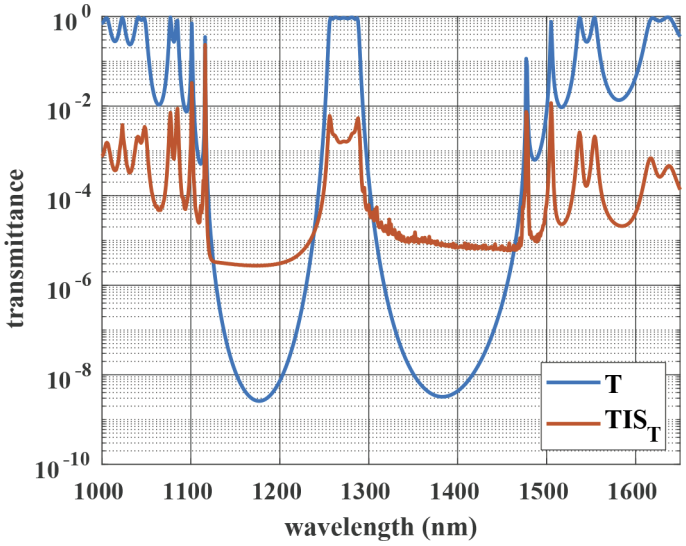

Fig. 3. Transmittance T and TIS_T values of the dedicated F1 band-pass filter in the near infrared.

Optics EXPRESS

is absolutely essential to control both specular and scattering properties at one and the same time. In this context, we propose here a hybrid approach which consists in using a *DNN* to refine and locally optimize existing complex multilayer structures. Starting from a design solution with respect to a specular constraint would be even more appropriate since the specular spectral response remains the key feature of most thin-film components. For this purpose, we have chosen a complex infrared bandpass filter F1 centered at 1273 nm, see Fig. 3.

This component has 60 layers of SiO_2 and Nb_2O_5, with thicknesses varying from around 140 nm to 1.14 µm. It is made of 6 superposed Fabry-Perot cavities. These cavities are composed of two $\lambda/4$ Bragg mirrors separated by a spacer, a layer of low index and thickness proportional to $\lambda/2$, where λ is the central wavelength of the Fabry-Perot. Figure 3 presents the specular transmission T and the transmitted TIS_T of this dedicated filter. Figure 4 presents the quarter-wavelength optical thickness (QWOT) of the layers at 1273 nm, namely the ratio between the effective thickness and the $\lambda/4$ value. The six cavities are clearly distinguishable from the layers composing the mirrors. The scattering levels are negligible compared to the transmittance, except for high rejection bands (around 1175 and 1385 nm) where the scattering level is higher than transmittance and could potentially alter the overall performance of the filter. We seek to optimize the structure such as to reduce the scattered light for these specific wavelength bands.

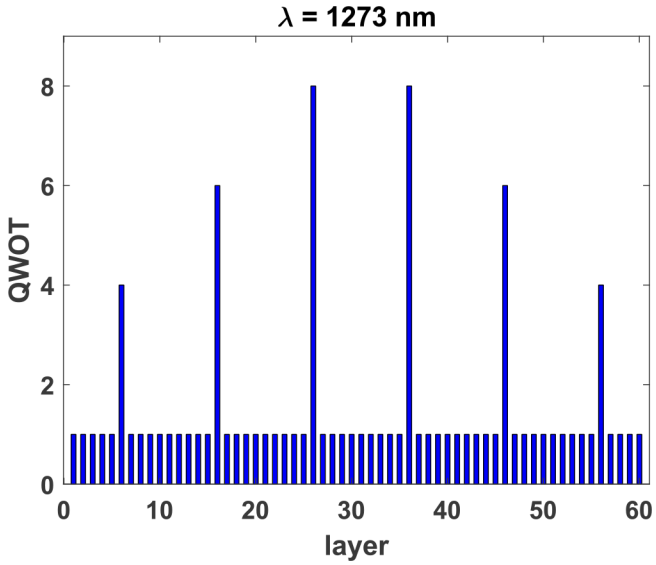

Fig. 4. Quarter Wavelength Optical Thickness of the F1 design at 1273 nm. The filter is made of 6 Fabry-Perot cavities, each one is composed of a spacer surrounded with Bragg mirrors.

The same *predictor* and *designer* framework is implemented but in this case the models do not deal with the exact thickness values of the layers but with thickness variations from the initial structure. Therefore, instead of working on thicknesses varying over a 1000 nm wide range, the thickness variations from the initial solution are smaller, so helping the learning process. The *predictor* has 6 hidden layers (respectively with 750, 750, 750, 500, 500 and 343 units), separated by leaky ReLU activations (leaky coefficient of 0.01). 75,000 examples are generated by altering the initial design structure with random noise (+/- 25 nm for each layer) and the associated spectral responses are computed. The whole generation process takes about 18 hours on our 24-core processor. The label output data sample both the scattering levels in the 1116-1478 nm band every 2 nm (182 points) and the transmittance in the 1256-1288 nm band every 0.2 nm (161 points). The model then learns scattering and transmittance responses at the same time with

Optics EXPRESS

output label data of 343 elements (182 + 161). The training is performed for 128 epochs, the final *RMSE* are 2.64 for the training set and 2.68 for the validation set.

The specular and light scattering properties are connected in such a way that it is impossible to modify only one of the two properties without affecting the other. Thus, reducing the scattering level might also affect the transmittance within the bandwidth. The target fixed for the *refinement* is the initial solution divided by 10 in the left-hand side rejection band (1125-1225 nm) and divided by 15 in the right-hand side rejection band (1300-1475 nm). This optimization criterion seeks to lower scattering values close to 10^{-6} in the two rejection bands. On the other hand, the transmittance target value is set to the initial value as the expectation is the same for this property. Figure 5 and Fig. 6 illustrate a compromise reached by the *designer* where the scattering level is reduced by half a decade in the left-hand side rejection band and one decade in the right-hand side rejection band. The out-of-band transmittance remains at acceptable levels and the in-band values are above 0.7 but show some critical oscillations that are not entirely acceptable for high performance filters.

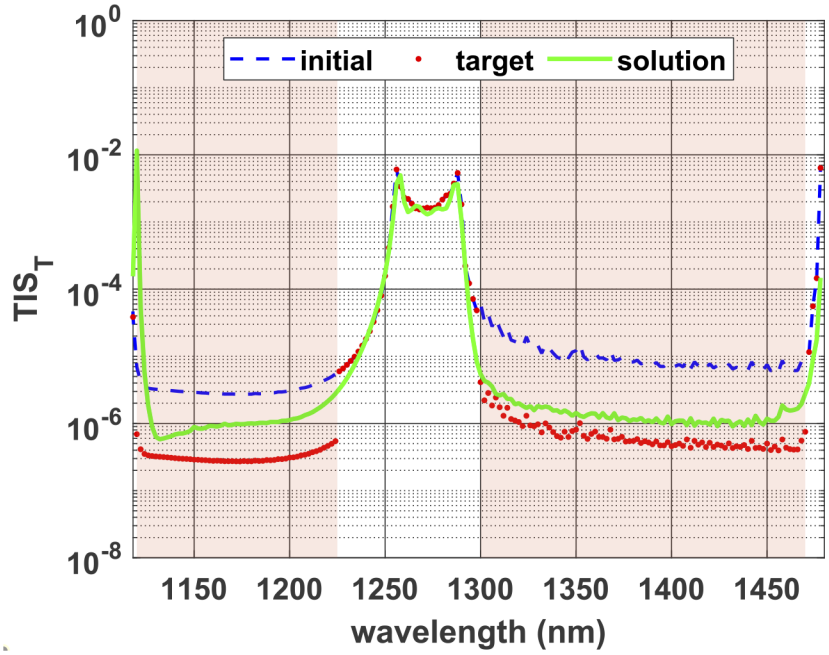

Fig. 5. Reduction of the TIS_T in the two rejection bands 1125-1225 nm and 1300-1475 nm.

The constraint is not fully satisfied. Table 1 compares the TIS_T values of the initial solution, the target, and the final solution at two wavelengths. The ratio between the *target* and the *initial solution* is $1/10$ at 1150 nm and $1/15$ at 1350 nm. At the end of the optimization process, the ratio between the *final solution* and the *initial solution* are respectively around $1/3$ and $1/9$. The reduction of the TIS_T is less than a decade but still shows some improvements.

Figure 7 presents the Quarter Wavelength Optical Thickness of the solution obtained after optimization, where we observe that the regular quarter wavelength structure is lost but the general pattern and the cavities remain. Further refinements of the optimized structure have not been successful. For that purpose, we have used a standard refinement procedure using the Optilayer software and have tried to correct the spectral oscillations on the specular response in the bandwidth. However, as our solution is unconventional, the classical means used to refine thin-film structures were inefficient. This whole approach is local and does not allow the

Optics EXPRESS

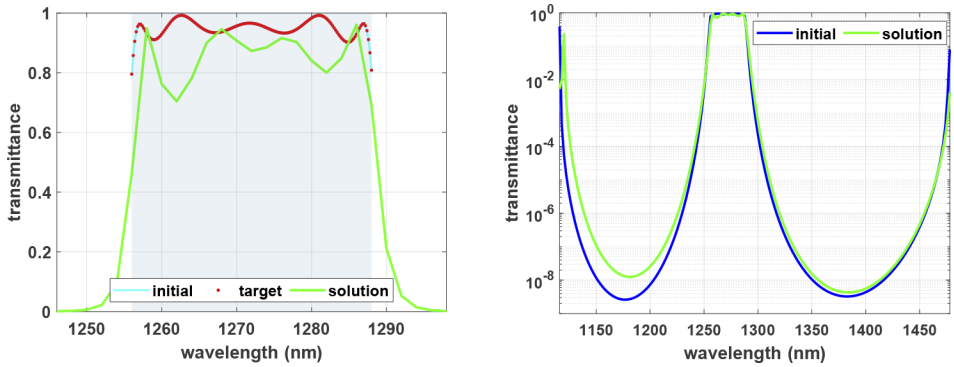

Fig. 6. Transmittance of the final solution. Left: bandwidth on a linear scale; only the wavelengths in the grey area are considered during the optimization process. Right: transmittance of the final solution on a broader wavelength range.

Table 1. Comparison of the TIS values of the initial solution, the target, and the final solution at 2 wavelengths

		@ 1150 nm	@1350 nm
initial solution		$2.89.10^{-6}$	$1.21.10^{-5}$
target		$2.89.10^{-7}$	$8.09.10^{-7}$
	ratio target/initial	1/10	1/15
final solution		$8.54.10^{-7}$	$1.38.10^{-6}$
	ratio final/initial	~ 1/3	~ 1/9

solution to be a global optimal because the parameters are adjusted closely around their initial values. It does, however, provide a good compromise between the overall specular and scattering performance of the component.

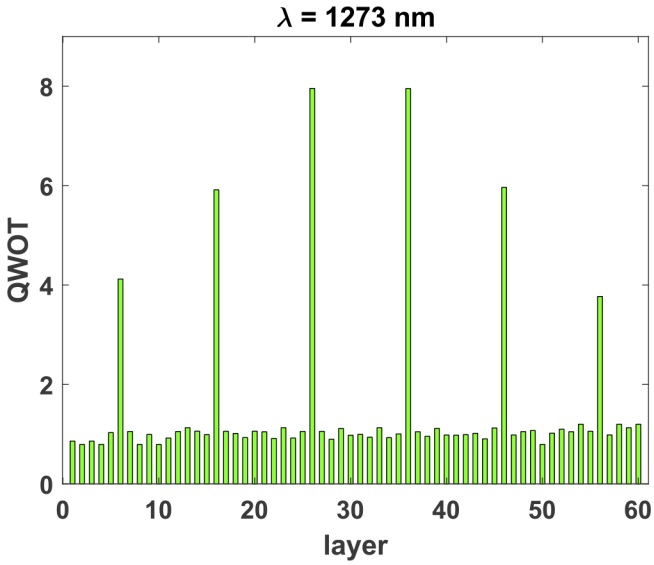

Fig. 7. Quarter Wavelength Optical Thickness (QWOT) of the final solution at 1273 nm. The final pattern looks like the initial one with a few variations on the layer thicknesses.

Optics EXPRESS

8. Conclusion

In this paper we have presented an optical thin-film design method based on light scattering properties and using deep neural networks. A first implementation handles simple 20-layer coatings and seeks to design optical responses from scratch. This approach is unlikely to lead to successful complex design and will probably fail to overcome current challenges. It also highlights the limitations in solving the inverse problem with this approach. A second implementation proposes the optimization of a far more complex component. The result of this local optimization is promising since we are able to reduce the scattering levels while allowing the transmittance to remain at acceptable values. However, the optimization still needs some improvements in order to explore further the scattering properties of multilayer thin-film components.

Funding. Centre National d'Etudes Spatiales.

Acknowledgements. The authors would like to thank CNES (Centre National d'Etudes Spatiales), CILAS ArianeGroup and LABTOP joint laboratory for funding this work.

Disclosures. The authors declare no conflicts of interest.

Data availability. Data underlying the results presented in this paper are not publicly available at this time but may be obtained from the authors upon reasonable request.

References

1. S. Reichel, R. Biertümpfel, U. Brauneck, S. Bourquin, and A. Marín-Franch, "Advanced astronomical filter design: challenges, strategy, and results to meet current and future requirements," in *Advances in Optical and Mechanical Technologies for Telescopes and Instrumentation II* (International Society for Optics and Photonics, 2016), Vol. 9912, p. 99122H.
2. J. A. Dobrowolski and B. T. Sullivan, "Universal antireflection coatings for substrates for the visible spectral region," Appl. Opt. **35**(25), 4993 (1996).
3. V. Pervak, C. Teisset, A. Sugita, S. Naumov, F. Krausz, and A. Apolonski, "High-dispersive mirrors for femtosecond lasers," Opt. Express **16**(14), 10220 (2008).
4. K. D. Hendrix, C. A. Hulse, G. J. Ockenfuss, and R. B. Sargent, "Demonstration of narrowband notch and multi-notch filters," in *Advances in Thin-Film Coatings for Optical Applications V* (International Society for Optics and Photonics, 2008), Vol. 7067, p. 706702.
5. T. Begou, F. Lemarchand, and J. Lumeau, "Advanced optical interference filters based on metal and dielectric layers," Opt. Express **24**(18), 20925 (2016).
6. K. Zhang, R. Huang, X. Tian, Y. Zhang, W. Huang, and C. Guan, "First-order nonparaxial scalar theory of surface and bulk scattering for high-quality optical coatings," J. Opt. Soc. Am. A **35**(11), 1823 (2018).
7. M. Zerrad, F. Lemarchand, S. Liukaityte, T. C. Begou, J. H. Lumeau, M. Lequime, and C. Amra, "Last improvements in large-angle scattering from complex optical coatings," in *Optical Interference Coatings 2016* (OSA, 2016), p. ThC.8.
8. J. Zhang, H. Wu, H. Jiao, S. Schröder, M. Trost, Z. Wang, and X. Cheng, "Reducing light scattering in high-reflection coatings through destructive interference at fully correlated interfaces," Opt. Lett. **42**(23), 5046 (2017).
9. R. L. Goff, H. Krol, C. Grèzes-Besset, M. Lequime, T. Bégou, C. Hecquet, M. Zerrad, B. Badoil, G. Montay, and K. Gasc, "Multispectral filters assemblies for earth remote sensing imagers," in *International Conference on Space Optics — ICSO 2014* (International Society for Optics and Photonics, 2017), Vol. 10563, p. 1056305.
10. P. D. Fuqua, T. Mooney, T. Mooney, J. D. Barrie, D. Rock, and H. I. Kim, "Angle Resolved Scattering from Optical Filters for Space Applications," in *Optical Interference Coatings (2010)*, Paper ThD1 (Optical Society of America, 2010), p. ThD1.
11. M. Fouchier, M. Zerrad, M. Lequime, and C. Amra, "Wide-range wavelength and angle resolved light scattering measurement setup," Opt. Lett. **45**(9), 2506–2509 (2020).
12. D. Vander-Hyde, C. Amra, M. Lequime, F. Magaña-Sandoval, J. R. Smith, and M. Zerrad, "Optical scatter of quantum noise filter cavity optics," Class. Quantum Grav. **32**(13), 135019 (2015).
13. S. Hild, H. Lück, W. Winkler, K. Strain, H. Grote, J. Smith, M. Malec, M. Hewitson, B. Willke, J. Hough, and K. Danzmann, "Measurement of a low-absorption sample of OH-reduced fused silica," Appl. Opt. **45**(28), 7269–7272 (2006).
14. F. Magaña-Sandoval, R. X. Adhikari, V. Frolov, J. Harms, J. Lee, S. Sankar, P. R. Saulson, and J. R. Smith, "Large-angle scattered light measurements for quantum-noise filter cavity design studies," J. Opt. Soc. Am. A **29**(8), 1722–1727 (2012).
15. T. Isogai, J. Miller, P. Kwee, L. Barsotti, and M. Evans, "Loss in long-storage-time optical cavities," Opt. Express **21**(24), 30114–30125 (2013).
16. J. R. Smith, R. X. Adhikari, K. M. Aleman, A. Avila-Alvarez, G. Billingsley, A. Gleckl, J. Guerrero, A. Markosyan, S. Penn, J. A. Rocha, D. Rose, and R. Wright, "Apparatus to Measure Optical Scatter of Coatings Versus Annealing

Optics EXPRESS

Temperature," in *Optical Interference Coatings Conference (OIC) 2019 (2019), Paper FA.2* (Optical Society of America, 2019), p. FA.2.
17. C. Padilla, P. Fritschel, F. Magaña-Sandoval, E. Muniz, J. R. Smith, and L. Zhang, "Low scatter and ultra-low reflectivity measured in a fused silica window," Appl. Opt. **53**(7), 1315–1321 (2014).
18. E. Capocasa, M. Barsuglia, J. Degallaix, L. Pinard, N. Straniero, R. Schnabel, K. Somiya, Y. Aso, D. Tatsumi, and R. Flaminio, "Estimation of losses in a 300 m filter cavity and quantum noise reduction in the KAGRA gravitational-wave detector," Phys. Rev. D **93**(8), 082004 (2016).
19. W. P. Kells, *Scattered Light Loss from LIGO Arm Cavity Mirrors* (2009).
20. G. Harry, T. P. Bodiya, and R. DeSalvo, *Optical Coatings and Thermal Noise in Precision Measurement* (Cambridge University, 2012).
21. V. Khodnevych, M. Lintz, N. Dinu-Jaeger, and N. Christensen, "Stray light estimates due to micrometeoroid damage in space optics, application to the LISA telescope," J. Astron. Telesc. Instrum. Syst. **6**(4), 048005 (2020).
22. N. Straniero, J. Degallaix, R. Flaminio, L. Pinard, and G. Cagnoli, "Realistic loss estimation due to the mirror surfaces in a 10 meters-long high finesse Fabry-Perot filter-cavity," Opt. Express **23**(16), 21455–21476 (2015).
23. D. G. Blair, M. Notcutt, C. T. Taylor, E. K. Wong, C. Walsh, A. Leistner, J. Seckold, J.-M. Mackowski, P. Ganau, C. Michel, and L. Pinard, "Development of low-loss sapphire mirrors," Appl. Opt. **36**(1), 337–341 (1997).
24. L. Pinard, B. Sassolas, R. Flaminio, D. Forest, A. Lacoudre, C. Michel, J. L. Montorio, and N. Morgado, "Toward a new generation of low-loss mirrors for the advanced gravitational waves interferometers," Opt. Lett. **36**(8), 1407–1409 (2011).
25. L. Pinard, P. Ganau, J.-M. Mackowski, C. Michel, M. Napolitano, E. Vireton, A. C. Boccara, V. Loriette, and H. Piombini, "Low loss DIBS mirrors 1064 nm for the VIRGO interferometer," in *Optical Interference Coatings Conference'95* (1995), Vol. 17, pp. 200–203.
26. F. Beauville, D. Buskulic, R. Flaminio, F. Marion, A. Masserot, L. Massonnet, B. Mours, F. Moreau, J. Ramonet, E. Tournefier, D. Verkindt, O. Veziant, M. Yvert, R. Barille, V. Dattilo, D. Enard, F. Fracsoni, A. Gennai, P. La Penna, M. Loupias, F. Paoeletti, L. Bracci, G. Calamai, E. Campagna, G. Conforto, E. Cuoco, I. Fiori, G. Guidi, G. Losurdo, F. Martelli, M. Mazzoni, B. Perniola, R. Stanga, F. Vetrano, A. Vicere, D. Babusci, G. Giordano, J. M. Mackowski, N. Morgado, L. Pinard, A. Remillieux, F. Acernese, F. Barone, E. Calloni, R. De Rosa, L. Di Fiore, A. Eleuteri, L. Milano, K. Qipiani, I. Ricciardi, G. Russo, S. Solimeno, M. Varvella, F. Bondu, A. Chassande-Mottin, F. Cleva, C. N. Man, F. Mornet, J. Pacheco, A. Pai, H. Trinquet, J. Y. Vinet, N. Arnaud, M. Barsuglia, M. A. Bizouard, V. Brisson, F. Cavalier, M. Davier, P. Hello, P. Heusse, S. Krecklberg, C. Boccara, V. Loriette, J. Moreau, V. Reita, P. Amico, L. Bosi, L. Gammaioni, M. Punturo, F. Travasso, H. Vocca, L. Barsotti, S. Braccini, C. Bradaschia, G. Cella, C. Corda, A. Di Virgilio, I. Ferrante, F. Fidecaro, A. Giazotto, E. Majorana, L. Holloway, R. Passaquieti, D. Passuello, R. Poggiani, A. Toncelli, M. Tonelli, L. Brocco, S. Frasca, C. Palomba, P. Puppo, P. Rapagnani, F. Ricci, and E. Brillet, "The VIRGO large mirrors: a challenge for low loss coatings," in *Edoardo Amaldi International Conference on Gravitational Waves 5* (IOP Publishing, 2003), Vol. 21, pp. S935–S945.
27. C. Amra, G. Albrand, and P. Roche, "Theory and application of antiscattering single layers: antiscattering antireflection coatings," Appl. Opt. **25**(16), 2695 (1986).
28. J. Zhang, H. Wu, I. V. Kozhevnikov, S. Shi, X. Cheng, and Z. Wang, "Interference suppression of light backscattering through oblique deposition of a layered reflecting coating: bi-layer on a substrate," Opt. Express **27**(11), 15262–15282 (2019).
29. C. Amra, M. Lequime, and M. Zerrad, *Electromagnetic Optics of Thin-Film Coatings: Light Scattering, Giant Field Enhancement, and Planar Microcavities* (Cambridge University, 2020).
30. P. Baumeister, "Design of Multilayer Filters by Successive Approximations," J. Opt. Soc. Am. **48**(12), 955–958 (1958).
31. H. A. Macleod, *Thin-Film Optical Filters*, 4th Edition (CRC, 2010).
32. A. V. Tikhonravov, M. K. Trubetskov, and G. W. DeBell, "Application of the needle optimization technique to the design of optical coatings," Appl. Opt. **35**(28), 5493–5508 (1996).
33. A. V. Tikhonravov, M. K. Trubetskov, and G. W. DeBell, "Optical coating design approaches based on the needle optimization technique," Appl. Opt. **46**(5), 704 (2007).
34. S. Martin, J. Rivory, and M. Schoenauer, "Synthesis of optical multilayer systems using genetic algorithms," Appl. Opt. **34**(13), 2247–2254 (1995).
35. C. You, C. T. Matyas, Y. Huang, J. P. Dowling, and G. Veronis, "Optimized Multilayer Structures With Ultrabroadband Near-Perfect Absorption," IEEE Photonics J. **12**(3), 1–10 (2020).
36. R. S. Hegde, "Accelerating optics design optimizations with deep learning," Opt. Express **58**(6), 065103 (2019).
37. M. A. Barry, V. Berthier, B. D. Wilts, M.-C. Cambourieux, P. Bennet, R. Pollès, O. Teytaud, E. Centeno, N. Biais, and A. Moreau, "Evolutionary algorithms converge towards evolved biological photonic structures," Sci. Rep. **10**(1), 12024 (2020).
38. R. I. Rabady and A. Ababneh, "Global optimal design of optical multilayer thin-film filters using particle swarm optimization," Optik **125**(1), 548–553 (2014).
39. C. P. Chang and Y. H. Lee, "Optimization of a thin-film multilayer design by use of the generalized simulated-annealing method," Opt. Lett. **15**(11), 595–597 (1990).
40. F. Lemarchand, "Application of clustering global optimization to thin film design problems," Opt. Express **22**(5), 5166 (2014).

Optics EXPRESS

41. D. Liu, Y. Tan, E. Khoram, and Z. Yu, "Training Deep Neural Networks for the Inverse Design of Nanophotonic Structures," ACS Photonics **5**(4), 1365–1369 (2018).
42. R. Unni, K. Yao, and Y. Zheng, "Deep Convolutional Mixture Density Network for Inverse Design of Layered Photonic Structures," ACS Photonics **7**(10), 2703–2712 (2020).
43. M. Zerrad, S. Liukaityte, M. Lequime, and C. Amra, "Light scattered by optical coatings: numerical predictions and comparison to experiment for a global analysis," Appl. Opt. **55**(34), 9680–9687 (2016).
44. M. A. Nielsen, "Neural Networks and Deep Learning," (2015).
45. J. Peurifoy, Y. Shen, L. Jing, Y. Yang, F. Cano-Renteria, B. G. DeLacy, J. D. Joannopoulos, M. Tegmark, and M. Soljačić, "Nanophotonic particle simulation and inverse design using artificial neural networks," Sci. Adv. **4**(6), eaar4206 (2018).
46. C. C. Nadell, B. Huang, J. M. Malof, and W. J. Padilla, "Deep learning for accelerated all-dielectric metasurface design," Opt. Express **27**(20), 27523–27535 (2019).
47. S. Molesky, Z. Lin, A. Y. Piggott, W. Jin, J. Vuckovic, and A. W. Rodriguez, "Outlook for inverse design in nanophotonics," Nat. Photonics **12**(11), 659–670 (2018).
48. S. So, T. Badloe, J. Noh, J. Bravo-Abad, and J. Rho, "Deep learning enabled inverse design in nanophotonics," Nanophotonics **9**(5), 1041–1057 (2020).
49. P. R. Wiecha, A. Arbouet, C. Girard, and O. L. Muskens, "Deep learning in nano-photonics: inverse design and beyond," Photonics Res. **9**(5), B182–B200 (2021).
50. J. Jiang, M. Chen, and J. A. Fan, "Deep neural networks for the evaluation and design of photonic devices," Nat. Rev. Mater **6**(8), 679–700 (2021).
51. W. Ma, Z. Liu, Z. A. Kudyshev, A. Boltasseva, W. Cai, and Y. Liu, "Deep learning for the design of photonic structures," Nat. Photonics **15**(2), 77–90 (2021).
52. W. Ma, F. Cheng, Y. Xu, Q. Wen, and Y. Liu, "Probabilistic Representation and Inverse Design of Metamaterials Based on a Deep Generative Model with Semi-Supervised Learning Strategy," Adv. Mater. **31**(35), 1901111 (2019).
53. Z. Liu, D. Zhu, S. P. Rodrigues, K.-T. Lee, and W. Cai, "Generative Model for the Inverse Design of Metasurfaces," Nano Lett. **18**(10), 6570–6576 (2018).
54. Z. A. Kudyshev, A. V. Kildishev, V. M. Shalaev, and A. Boltasseva, "Machine-learning-assisted metasurface design for high-efficiency thermal emitter optimization," Appl. Phys. Rev. **7**(2), 021407 (2020).
55. D. Zhu, Z. Liu, L. Raju, A. S. Kim, and W. Cai, "Building Multifunctional Metasystems via Algorithmic Construction," ACS Nano **15**(2), 2318–2326 (2021).
56. M. Trubetskov, "Deep search methods for multilayer coating design," Appl. Opt. **59**(5), A75 (2020).
57. L. Gao, F. Lemarchand, and M. Lequime, "Exploitation of multiple incidences spectrometric measurements for thin film reverse engineering," Opt. Express **20**(14), 15734 (2012).
58. L. Gao, F. Lemarchand, and M. Lequime, "Refractive index determination of SiO_2 layer in the UV/Vis/NIR range: spectrophotometric reverse engineering on single and bi-layer designs," JEOS:RP **8**, 13010 (2013).
59. C.-T. Chen and G. X. Gu, "Generative Deep Neural Networks for Inverse Materials Design Using Backpropagation and Active Learning," Adv. Sci. **7**(5), 1902607 (2020).